Journal of ELECTRONIC MATERIALS, Vol. 48, No. 11, 2019
https://doi.org/10.1007/s11664-019-07565-0
© 2019 The Minerals, Metals & Materials Society

Characterization of Aluminum Contacts on Cobalt Oxide Films Grown with Different Oxygen Concentrations

JOÃO C. ANGELICO ,[1,2,3] NILTON F.A. NETO,[1] and JOSÉ H. DIAS DA SILVA[1]

1.—Universidade Estadual Paulista - UNESP, Bauru, São Paulo 17033-360, Brazil. 2.—Universidade Paulista - UNIP, Bauru, São Paulo 17048-290, Brazil. 3.—e-mail: jcangelico@gmail.com

The electronic transport in a metal/semiconductor/metal (MSM) structure, consisting of cobalt oxide films with aluminum (Al) contacts, was investigated. The cobalt oxides were grown by direct current (DC) magnetron sputtering using different oxygen gas flow rates. The behavior of the electric conductivity in the 200 K–350 K temperature range, the Schottky barrier heights ($\emptyset_B$) and specific contact resistances (R_c) were investigated. The analysis shows that small oxygen flow variations produce significant changes in electrical characteristics of the MSM structure.

Key words: Schottky barrier, thin films, electrical conductivity

INTRODUCTION

Polycrystalline semiconductors have been intensively studied in recent decades owing to their potential for applications in low-cost electronic devices requiring high stability and efficiency, such as solar cells and thin film transistors. Among these, cobalt oxides are highly attractive for applications in catalysis[1,2], gas sensors,[3] electrodes in lithium-ion batteries[4,5], construction of capacitors,[6] and photovoltaic cells.[7,8]

Understanding the mechanisms of electronic transport in polycrystalline cobalt oxide films is fundamental to broaden and improve the application of these materials in devices. However, the electronic transport in these materials is considerably complex owing to the small dimensions of the crystallites that produce a high density of grain boundaries per unit volume, reducing the average electronic mobility.[9] In addition to the complexity of the electronic interactions between the metal and oxygen ions in the Co_3O_4 and CoO regular crystalline structures, the structural irregularities present in the polycrystalline cobalt oxide films, must also be considered.[10,11] The electrostatic interactions between the metallic cobalt and oxygen, together with the structural irregularities, enable the existence of a large density of defect levels in the material. The electronic transitions between these levels define the electrical conductivity mechanisms. Hence, electrical, optical, and structural measurements must be complemented in the study of electronic transport in cobalt oxide films.[10–15]

The electronic transport at the metal-semiconductor interface is also of paramount importance because the link between the electronic device built with a cobalt oxide film and the remainder of the circuit is made through metallic electrical contacts. In this work, the electrical conductivity of aluminum/Co_3O_4/aluminum (Al/Co_3O_4/Al) and aluminum/CoO/aluminum (Al/CoO/Al) structures were studied in polycrystalline films grown by direct current (DC) magnetron sputtering with different concentrations of oxygen.

EXPERIMENTAL PROCEDURE

The cobalt oxide films were grown using a cobalt metal target (99.95%) in an atmosphere composed of a mixture of argon (99.9999%) and oxygen (99.9999%), using silica glass substrates in a Kurt J. Lesker, System I, sputtering equipment. Before depositions, the substrates were carefully cleaned,

(Received March 30, 2019; accepted August 14, 2019; published online August 26, 2019)

dried, and fed to the system.[16] In a residual pressure of 4×10^{-7} kPa, substrates were heated and kept at 720 ± 10 K during the growth of the films. Different oxygen flow rates, measured in standard cubic centimeters per minute (sccm), using an electronic MKS model 247 flow controller, were used for each sample: 1.00 ± 0.05 sccm (sample label A), 1.50 ± 0.05 sccm (sample label B), 2.50 ± 0.05 sccm (sample label C), and 5.00 ± 0.05 sccm (sample label D), while the Ar flow rate kept at 40 sccm in all depositions. The deposition power (80 W) and total pressure (6.6×10^{-4} kPa) were kept constant. The deposition parameters are presented in Table I.

The structural characterization of the films was performed using a Panalytical Empyrean diffractometer with $CuK\alpha$ radiation ($\lambda = 1.54060$Å) using the $\theta-2\theta$ configuration at a measuring range of 15° to 80° with a pitch of 0.01°.

The absorbance spectra in the UV/Vis/NIR region were obtained with a Perkin Elmer Lambda 1050 spectrophotometer. Measurements were made in the 250 nm–2500 nm range.

Parallel aluminum electrical contacts, 10 mm in length, spaced at 1 mm, 1.5 mm and 2.0 mm, were deposited by thermal evaporation in vacuum (residual pressure 2×10^{-7} kPa) on the film surfaces using shadow masks. The contacts were patterned at different distances to measure the specific contact resistance using the transmission-line method (TLM).[17] Electrical connection wires were welded with silver epoxy (EPOTEK H20E) to the aluminum contacts.

Measurements of the current versus voltage characteristics ($I \times V$) and the conductivity as a function of the inverse of the temperature ($\sigma \times 1/T$), in the 200 K and 350 K range were performed in vacuum ($\sim 10^{-7}$ kPa) using a Janis cryostat, model CCS - 400/204, connected to a LakeShore 335 temperature controller. The electrical signals were measured with a Keithley 6517A electrometer. The experiments were controlled by GPIB interface (National Instruments GPIB - IEEE 488.2) connected to a desktop computer. A specially developed MATLAB program was used in the experiment control and data collection.

Table I. Deposition parameters of films prepared by DC sputtering

Sample Label	O_2 flow (sccm)	Phase
A	1.0	CoO[a]
B	1.5	CoO
C	2.5	Co_3O_4
D	5.0	Co_3O_4

The constant parameters used during deposition were DC power, 80 W; substrate temperature, ~720 K; deposition time, 66 min; Ar flow, 40 sccm; pressure, 6.6×10^{-4} kPa.
[a]It presented metallic characteristics in the absorbance spectrum.

RESULTS AND DISCUSSION

The x-ray diffractograms of samples A, B, C, and D display the structural evolution (Fig. 1) of the films with the variation of the oxygen supply. It can be observed that the films deposited with 1.0 sccm (sample A) and 1.5 sccm (sample B) present only the cubic rock-salt CoO phase. For 2.5 sccm (sample C) and 5.0 sccm (sample D) flow rates, the cubic spinel Co_3O_4 phase is predominant.

Figure 2 displays the absorption spectra of samples A, B, C, and D. Sample A presented the highest absorption in the near-infrared region. For wavelengths ranging from 750 nm to 2500 nm, the mean transmittance of this sample was approximately 20%, indicating that the film has a metallic

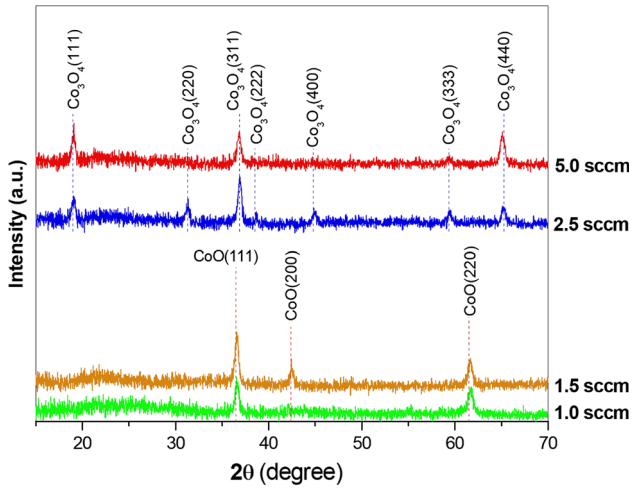

Fig. 1. X-ray diffractogram of samples deposited with different oxygen flows.

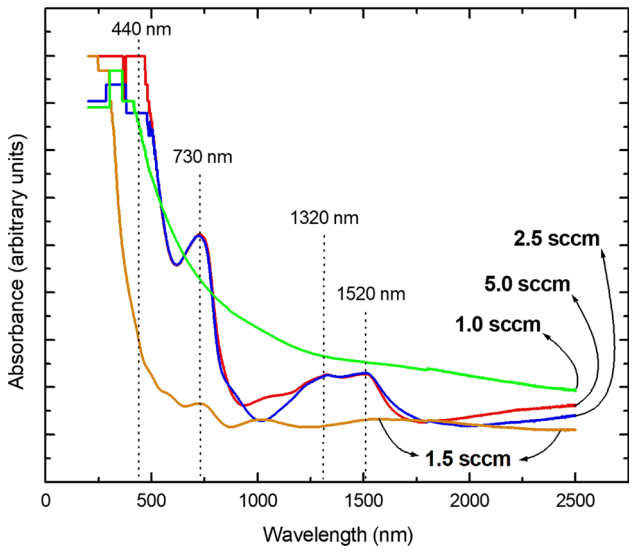

Fig. 2. Absorbance spectra of samples deposited with different oxygen flows.

character. In sample B (1.5 sccm), the absence of absorption bands about 1320 nm and 1520 nm, attributed to *Co 3d* transitions in the Co_3O_4 spinel crystals,[18] indicates the predominance of the cubic rock-salt CoO phase, which had been previously identified in the x-ray diffraction measurements (Fig. 1). In the absorption spectra of samples C and D, absorption bands in the near-infrared range are observed; these are related to the *3d* states of the Co^{2+} and Co^{3+} ions located in the octahedral and tetrahedral sites of the Co_3O_4 spinel structure, respectively.[18] These results are also consistent with the x-ray diffraction measurements, which indicated a predominance of the Co_3O_4 phase in the films grown with oxygen flows of 2.5 sccm and 5.0 sccm (samples C and D).

Figure 3 displays the electrical conductivity of the metal-semiconductor-metal (MSM) structure of samples A, B, C, and D in the temperature range 200 K to 330 K. It was not possible to measure the conductivities of samples A and B below 200 K. This problem is due to the relatively large distance between contacts and to the low conductivities of the films.

The electrical conductivity was the highest in the film with the highest O_2 flow rate (5.0 sccm, sample D). This counter intuitive behavior can be attributed to two components. The first, as pointed out by Cheng et al. [19], can be due to structural and morphological changes produced in the polycrystalline Co_3O_4 films. Similarly to the observed by Cheng et al. the x-ray diffraction peak (311) of the film grown with 2.5 sccm (sample C) presents greater intensity than that observed in the sample D (Fig. 1). The dominant peak in the plane (311) indicates an asymmetry in the structure, causing greater spacing between the Co^{2+} and Co^{3+} ions, which can reduce the conductivity attributed to polaronic hopping of holes.[19] A second contribution

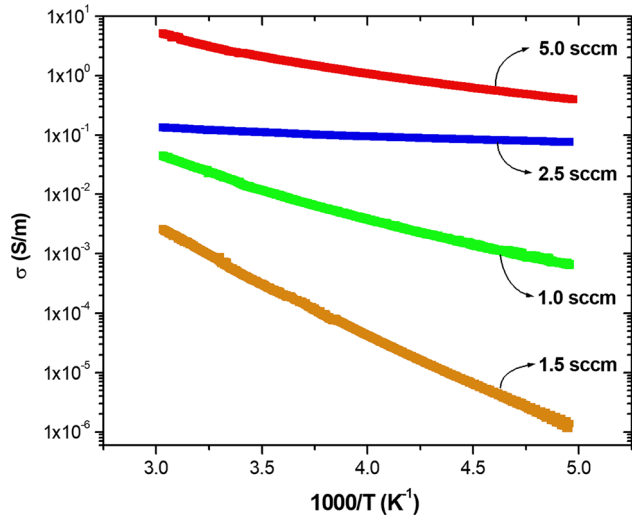

Fig. 3. Measurements of conductivity as a function of the temperature of samples deposited with different oxygen flows.

can be attributed to a larger amount of Co vacancies, and consequently to a higher hole density in the oxygen rich spinel structure. These are possibly the factor that determines the lower conductivity of sample C in relation to sample D.

When the O_2 flow is reduced to 1.5 sccm (Sample B), the electrical conductivity is significantly decreased and reaches the lowest value in the set in the analyzed temperature range. This decrease in electrical conductivity is associated with the phase transition from Co_3O_4 to CoO. The reduction of electrical conductivity with the decrease of the oxygen flow was not observed for sample A (grown with 1.0 sccm). This behavior is attributed to the metallic character of sample A produced by the low oxygen supply. This metal character of sample A is apparent in its absorbance spectrum shown in Fig. 2.

Measurements $I \times V$ for the MSM system, at room temperature, are presented in Fig. 4. It can be observed that for sample A (1.0 sccm) the aluminum contacts did not present ohmic behavior, whereas the curve obtained for sample B (1.5 sccm) indicates a small deviation of the ohmic behavior at low voltage only. Sample C (2.5 sccm) presented ohmic behavior in the voltage range -2 V to 2 V. A deviation from linear can also be observed in sample D (5.0 sccm), indicating a non-ohmic behavior, similar to that of sample A.

The different results observed in the $I \times V$ curves are related to the potential barriers formed between the metal and semiconductor (Schottky effect). The MSM structure should be analyzed as two opposing Schottky barriers (placed back-to-back). Thermionic emission is the dominant process when a low voltage is applied. With increasing voltage, quantum tunneling becomes the dominant mechanism. The electronic current through the MSM structure is limited by the reverse-biased contact. According to the thermionic emission theory, the reverse current density in an ideal Schottky diode must saturate in[20]:

$$J_o = AT^2 \exp\left(\frac{-q\emptyset_B}{kT}\right), \tag{1}$$

where A is the Richardson constant, T is the temperature, k is the Boltzmann constant, q is the elementary electric charge, and $\emptyset_B$ is the height of the potential barrier which is a decreasing function of the applied reverse bias. For large values of the reverse applied bias $\Delta\emptyset_B$ is given by[21]:

$$\Delta\emptyset_B \approx C^{1/4}V^{1/4}, \tag{2}$$

where C is related to the carrier density and permittivity of the semiconductor. The current density for the MSM structure can be estimated by[21]:

$$J = J_o \exp\left(q\frac{\Delta\emptyset_B}{kT}\right) = J_o \exp\left(q\frac{C^{1/4}V^{1/4}}{KT}\right). \tag{3}$$

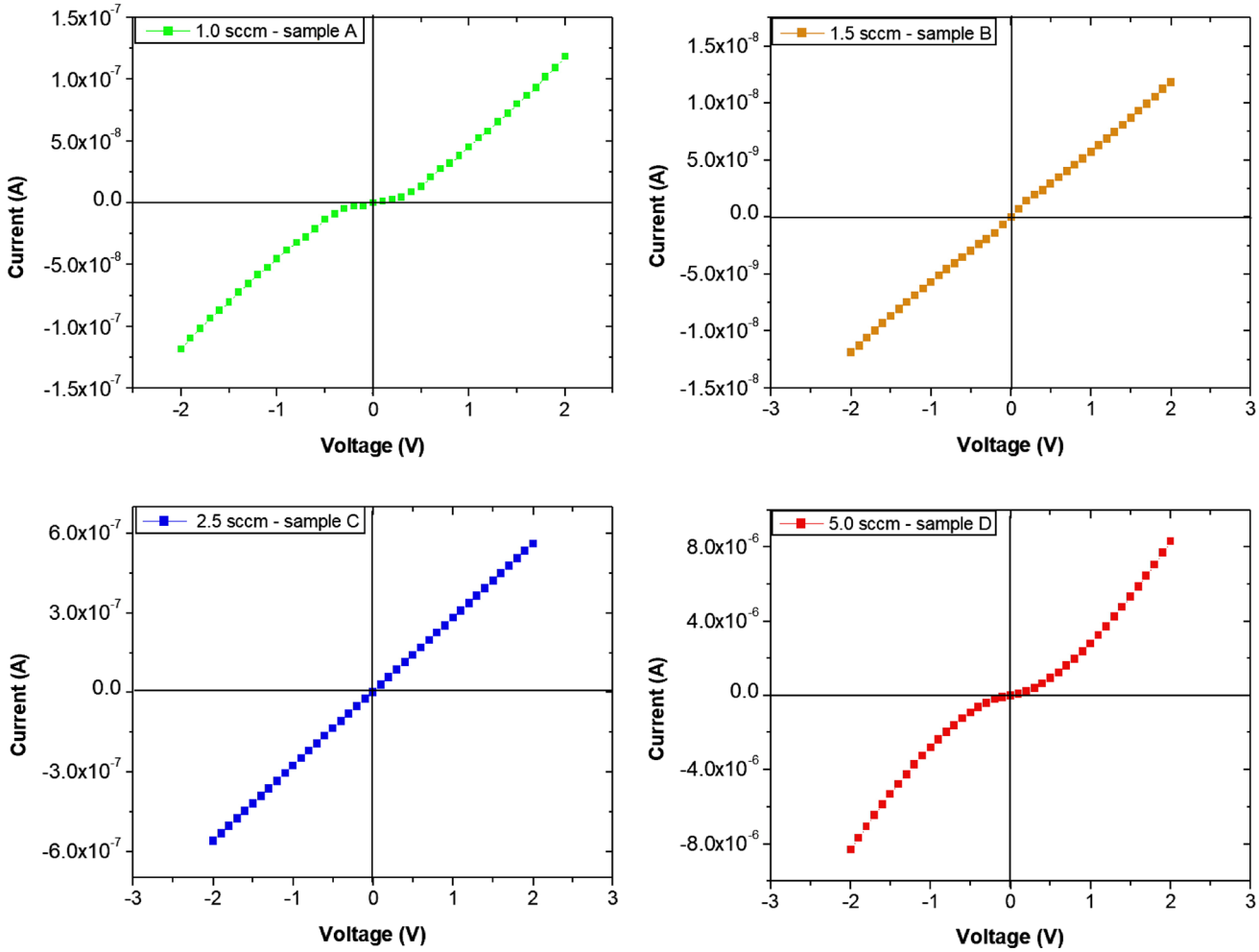

Fig. 4. Current-voltage ($I \times V$) plot of the samples deposited with different oxygen flows.

For a given temperature, J_o can be obtained from the intersection with the current density axis in a plot of $\ln J$ as a function of $V^{1/4}$. It is possible to obtain the value of J_o for different temperatures by measuring the current density at each of these temperatures. Plotting $\ln\left(J_o/T^2\right)$ as a function of T^{-1}, according to Eq. 1, it is possible to obtain $\emptyset_B$ from the slope of the line. When determining $\emptyset_B$, care must be exercised to work with low voltage values and high temperatures to ensure that the thermionic emission is the dominant transport mechanism.[21]

Figure 5 displays a plot of $\ln J$ as a function of $V^{1/4}$ for the 290 K, 320 K, and 350 K temperatures obtained from the $I \times V$ data of sample D. The inset of Fig. 5 presents a plot of $\ln\left(J_o/T^2\right)$ as a function of the inverse of the temperature and the respective $\emptyset_B$ value obtained from the angular coefficient of the line.

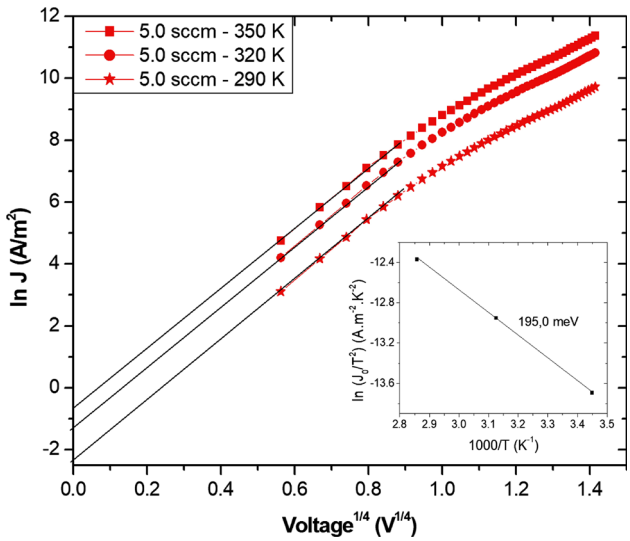

Fig. 5. Plot of $\ln(J)$ as function of $V^{1/4}$ for sample deposited with an oxygen flow of 5.0 sccm. Inset: plot of $\ln\left(J_o/T^2\right)$ as a function of T^{-1}.

Proceeding analogously for samples A, B, and C, the heights of the potential barriers listed in Table II were obtained.

Considering that the electrical resistance of the contact with the film is directly proportional to the height of the potential barrier $\emptyset_B$, we used the transmission-line method to analyze the specific contact resistance. The technique requires the formation of contacts with controlled geometry and evaluates the difference in resistance between equally sized pairs of contacts separated by different distances.[17] The specific contact resistance (R_c) is calculated from a measurement of the effective contact resistance (R_0), the contact width (W), and the transfer length (L_T):

$$R_c = R_0 W L_T. \quad (4)$$

Figure 6 displays the measured resistance against the contact separation for sample D (5.0 sccm). The following values can be observed in this figure: $2R_0 = 3000\Omega$ and $2L_T = 1.2 \times 10^{-5}$ m. With the aid of Eq. 4, for a contact width equal to 1×10^{-3} m, we obtain $R_c = 9 \times 10^{-6}$ Ω m^2. Proceeding in analogously for samples A, B, and C, the specific contact resistance (R_c) listed in Table II were obtained.

The surface morphology of the films makes it difficult to determine the areas of the contacts (W), limiting the accuracy of the determination of the specific contact resistance. Even with this difficulty, the values obtained for the specific contact resistances in the samples grown with different oxygen flows are proportional to the Schottky barrier height (Table II).

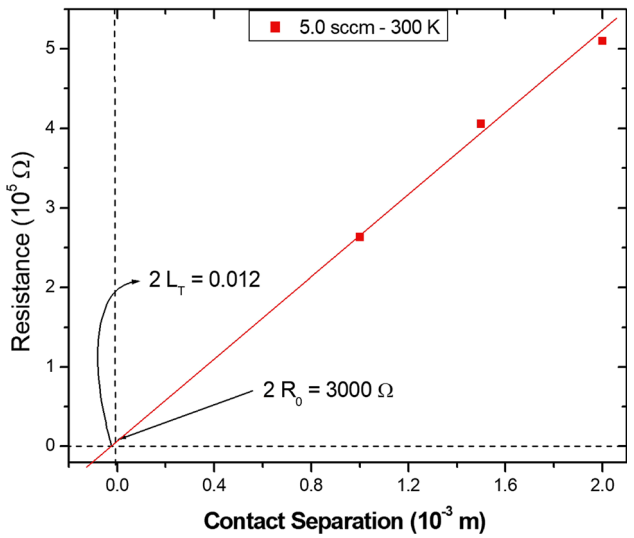

Fig. 6. Evaluation of the specific contact resistance of Al contacts using the transmission-line method.

Table II. Schottky barrier height ($\emptyset_B$) and specific contact resistance (R_c) for samples grown with different oxygen concentration

Sample label	O_2 flux (sccm)	$\emptyset_B$ (meV)	R_c (Ω m^2)
A	1.0	180.0	3×10^{-6}
B	1.5	70.0	2×10^{-7}
C	2.5	30.0	5×10^{-8}
D	5.0	195.0	9×10^{-6}

The metal and semiconductor work functions are determinant in the characteristics of the metal/semiconductor contact, although the formation of alloys and/or interdiffusion at the junction can have a strong influence.[22–24] The ohmic (or non-ohmic) behaviour in the metal/semiconductor junction can be evaluated with the aid of the parameter $\Delta = \frac{1}{2}E_g - \emptyset_m + \emptyset_S$, with E_g being the gap energy, $\emptyset_m$ the metal work function, and $\emptyset_S$ the semiconductor work function.[25,26] For p-type semiconductors (hot tip thermopower measurements indicated that the cobalt oxide films studied in this work are of type p), the metal-semiconductor contact is ohmic when the value of the parameter Δ is negative and non-ohmic for positive values. As the average work function of aluminum is 4.17 eV and the Co_3O_4 work function varies between 4.30 eV and 4.50 eV [27], the parameter Δ will always have positive values for any value of gap energy (E_g), suggesting a non-ohmic contact for the Al/Co_3O_4 junction, in accordance with the result of Fig 4 (sample D).

The oxidative state of the metal oxides changes the electronegativity of the cations, causing the work function of these oxides to be dependent on the chemical and structural factors. The metal-oxide work function decreases with oxygen deficiency.[28] This explains the ohmic behavior of sample C (Fig. 4), which despite having a predominantly cubic spinel Co_3O_4 phase, had a reduced work function owing to the lower oxygen flow provided during the deposition process.

Owing to the reduction of oxygen flow to 1.5 sccm, sample B presented the cubic rock-salt CoO phase, as indicated by the x-ray diffraction measurements (Fig. 1) and absorption (Fig. 2). For this reason, the Al/CoO contact of sample B did not present ohmic behavior (Fig. 4). When the oxygen flow was reduced to 1.0 sccm, the film presented metallic characteristics, as indicated by the absorption spectra (Fig. 2). The work function of metallic Co is approximately 5.00 eV,[27] making the parameter $\Delta = \frac{1}{2}E_g - \emptyset_m + \emptyset_S$ positive, and implying a non-ohmic contact as displayed in Fig. 4 (sample A). These results show that the variation in oxygen flow in the growth process of cobalt oxide films by sputtering enables obtaining different values of Schottky barrier between these films and the aluminum contacts.

CONCLUSIONS

Cobalt oxide films grown with O_2 flow rates of 2.5 sccm and 5.0 sccm, at a constant power of 80 W, presented cubic spinel Co_3O_4 as the predominant phase, whereas the films grown with flows of 1.0

sccm and 1.5 sccm presented a rock-salt CoO phase. The electrical behavior of the MSM structure has significantly changed for each O_2 flow, despite the phase similarity of the oxide films noticed in the low O_2 and high O_2 flow ranges. This result attests the high sensitivity of the electrical characteristics to small O_2 variations.

Among other effects, the work function of the films increased when the transition from the Co_3O_4 to the CoO phase occurred. For this reason, the aluminum contacts did not present ohmic behavior in the rock-salt CoO films grown (1.0 sccm and 1.5 sccm oxygen flow rates).

In the $Al/Co_3O_4/Al$ MSM structures, the Schottky barrier heights were demonstrated to be lower in films grown with 2.5 sccm than in the ones grown with 5.0 sccm oxygen flow rates. In the former, the $I \times V$ curves indicated ohmic behavior in the $-$ 2.0 to 2.0 V range. This result was related to the smaller value of the work function of the films grown using 2.5 sccm and was attributed to oxygen deficiency during the growth process.

ACKNOWLEDGEMENTS

Authors acknowledge Douglas M. G. Leite and Cristiane Stegemann for x-ray diffraction measurements (FINEP – Grant 01.13.0328.00), and the financing from FAPESP (Grant 2017/18916-2) and UNIP (scholarship 7-03-1055/2017).

REFERENCES

1. L. Cao, Y. Cao, X. Liu, Q. Luo, W. Liu, W. Zhang, X. Mou, J. Yang, T. Yao, and S. Wei, *J. Mater. Chem.* 6, 15684 (2018).
2. Y. Zu, P. Yang, J. Wang, X. Liu, J. Ren, G. Lu, and Y. Wang, *Appl. Catal. B.* 146, 244 (2014).
3. Z. Wen, L. Zhu, W. Mei, L. Hu, Y. Li, L. Sun, H. Cai, and Z. Ye, *Sens. Actuators, B.* 186, 172–179 (2013).
4. P. Poizot, S. Laruelle, S. Grugeon, L. Dupont, and J.-M. Tarascon, *Nature.* 407, 496 (2000).
5. A.K. Rai, L.T. Anh, J. Gim, and J. Kim, *Ceram. Int.* 39, 9325 (2013).
6. S.G. Kandalkar, J.L. Gunjakar, and C.D. Loklande, *Appl. Surf. Sci.* 254, 5540 (2008).
7. C. Lohaus, J. Morasch, J. Brötz, A. Klein, and W. Jaegermann, *J. Phys. D Appl. Phys.* 49, 155306 (2016).
8. B. Kupfer, K. Majhi, D.A. Keller, Y. Bouhadana, S. Rühle, H.N. Barad, A.Y. Anderson, and A. Zaban, *Adv. Energy Mater.* 5, 1401007 (2015).
9. P.S. Patil, L.D. Kadam, and C.D. Lokhande, *Thin Solid Films.* 272, 29 (1996).
10. S. Thota, A. Kumar, and J. Kumar, *Mater. Sci. Eng., B.* 164, 30 (2009).
11. G. St, M. Christoskova, M. Stoyanova, and D. Georgieva, Mehandjiev. *Mater. Chem. Phys.* 60, 39 (1999).
12. H.K. Lin, H.C. Chiu, H.C. Tsai, S.H. Chien, and C.B. Wang, *Catal. Lett.* 88, 169 (2003).
13. K.M.E. Miedzinska, B.R. Hollebone, and J.G. Cook, *J. Phys. Chem. Solids.* 48, 649 (1987).
14. M.C. Biesinger, B.P. Payne, A.P. Grosvenor, L.W.M. Lau, A.R. Gerson, and R.St.C Smart, *Appl. Surf. Sci.* 257, 2717 (2011).
15. J. Chen, X. Wu, and A. Selloni, *Phys. Rev. B.* 83, 245204 (2011).
16. N.F. Azevedo Neto, D.M.G. Leite, P.N. Lisboa-Filho, J.H.D. da Silva, and J. Vac, *Sci. Technol. A.* 6, 36 (2018).
17. B.L. Sharma, ed., *Metal-Semiconductor Schottky Barrier Junctions and Their Applications* (New York: Plenum Press, 1984).
18. L. Qiao, H.Y. Xiao, H.M. Meyer, J.N. Sun, C.M. Rouleau, A.A. Puretzky, D.B. Geohegan, I.N. Ivanov, M. Yoon, W.J. Weber, and M.D. Biegalski, *J. Mater. Chem.* 1, 4628 (2013).
19. C.S. Cheng, M. Serizawa, H. Sakata, and T. Hirayama, *Mater. Chem. Phys.* 53, 225 (1998).
20. S.M. Sze, *Physics of Semiconductor Devices* (Hoboken: Wiley, 1981).
21. E.H. Rhoderick and R.H. Williams, *Metal-semiconductor contacts* (Oxford: Clarendon, Oxford University Press, 1988).
22. N. Yildirim, A. Turut, and V. Turut, *Microelectron. Eng.* 87, 2225 (2010).
23. T. Kim and D.D.L. Chung, *Thin Solid Films.* 147, 177 (1987).
24. T.S. Kuan, P.E. Batson, T.N. Jackson, H. Rupprecht, and E.L. Wilkie, *J. Appl. Phys.* 54, 6952 (1983).
25. B. Varghese, B. Mukherjee, K.R.G. Karthik, K.B. Jinesh, S.G. Mhaisalkar, S.E. Tok, and C.H. Sow, *J. Appl. Phys.* 111, 104306 (2012).
26. B. Klingenberg, F. Grellner, D. Borgmann, and G. Wedler, *Surf. Sci.* 296, 374 (1993).
27. D.R. Lide, ed., *CRC Handbook of Chemistry and Physics*, 84th ed. (CRC Press LLC, 2003–2004).
28. M.T. Greiner, L. Chai, M.G. Helander, W. Tang, and Z. Lu, *Adv. Funct. Mater.* 22, 4557 (2012).

Publisher's Note Springer Nature remains neutral with regard to jurisdictional claims in published maps and institutional affiliations.